Design Optimization and Analysis of Single-Sided Linear Induction Motor, Considering All Phenomena

A. Shiri, *Student Member, IEEE*, and A. Shoulaie

***Abstract*—Regarding the different capabilities, linear motors have been employed in many applications in industry. Among different linear motors, single-sided linear induction motors (SLIMs) have been widely used due to their simplicity and low construction cost. However, these types of motors suffer from low efficiency and power factor and also, existence of so called end effect. The end effect produces braking force that deteriorates the performance of the motor, especially at high speeds. In this paper, analytical equations are derived for end effect braking force, efficiency, power factor, and output thrust. Employing the derived equations and considering all phenomena involved in the single-sided SLIM, a simple design procedure is presented and the effect of different design variables on the performance of the motor is analyzed. A multiobjective optimization method based on genetic algorithm is introduced to maximize efficiency and power factor, as well as to reduce primary weight and end effect braking force, simultaneously. All effective design variables are considered in optimization. The results show significant improvements in the objective function. Finally, the 2-D and 3-D finite element method is employed to validate the results obtained by the analytical method.**

***Index Terms*—Efficiency, end effect braking force, genetic algorithm, magnetic air-gap, optimization, power factor, thrust.**

I. Introduction

In recent three decades, linear electric motors have been used in industry applications. These kinds of motors are capable of producing linear motion without any need for transmission system and mechanical gears. Among various types of linear motors, linear induction motors (LIMs) have gained interests of researchers due to their simple structure. So, many investigations are devoted to these kinds of motors [1]–[8]. There are different types of LIMs, among them, single-sided linear induction motors (SLIMs) are widely used in transportation systems [9]–[12]. Different parameters are involved in designing SLIMs. These parameters affect the performance of the machine in different manners. Increasing a certain parameter may increase an output, at the same time, it may decrease another one. So, the proper performance of the SLIMs requires optimization of their design, regarding different outputs as objective functions.

In order to optimize the LIM, different objective functions have been introduced in the literature. In [13], the primary weight has been considered as objective function. In other research, the thrust and power to weight ratio are maximized [14]. In [15] and [16], the optimum winding design of LIM has been considered. Isfahani *et al*., have optimized the LIM to have maximum efficiency and power factor [17], [18]. In the latter works, only the primary current density, the motor slip, the primary width to pole pitch ratio, and the secondary aluminum sheet thickness have been selected as design independent variables; while the air-gap, frequency, and other important parameters that are crucial in designing SLIM, are not considered in the optimization. In addition, the phenomena such as "end effect" and "edge effect" are not involved. So, the design could be reliable in only low speed motors. A similar work has been done in [19] using imperialist competitive algorithm. Recently, Bazghaleh *et al*., included end effect phenomenon in design by defining end effect factor [20]. The end effect factor in this reference has been defined by the differences of the air-gap power with and without end effect. There are some research works that investigate the end effect in LIMs. In [21], the existence of the end effect has been confirmed by using analytical equations and defining end effect factor. Also, the effect of design parameters on the end effect have been investigated in [22]–[24]. In the literature, end effect braking force (EEBF) has not been considered in design by researchers while it has determinant effects on the performance of the SLIM. In this paper, based on Duncan equivalent circuit model [25], analytical equations for the EEBF, output thrust and efficiency are derived. Then, considering EEBF, a computer-aided systematic and applicable design algorithm is proposed for SLIM. In the proposed algorithm, all phenomena of the LIM are taken into account. Finally, Genetic algorithm-based multiobjective design optimization is done to maximize the efficiency and power factor, as well as to minimize EEBF and primary weight, considering all design variables that are effective in the performance of the motor. To confirm the validity of the proposed design, as well as analytically obtained outputs, finite element method (FEM) is employed and the results are compared.

II. Equivalent Circuit Model of SLIM

Similar to rotary induction motors, the performance of SLIM can be investigated by equivalent circuit model [25]–[28]. For the design of the SLIM shown in Fig. 1, the equivalent circuit model proposed by Duncan is employed [25]. The per-phase equivalent circuit model of SLIM is shown in Fig. 2. In this figure, R_1 is the per-phase resistance of the primary that is calculated as follows:

$$R_1 = 2(W_s + l_{\rm ec})N/(\sigma_w A_w). \quad (1)$$

Manuscript received October 15, 2011; revised February 3, 2012; accepted March 2, 2012. Date of publication April 26, 2012; date of current version May 18, 2012. Paper no. TEC-00537-2011.

The authors are with the Department of Electrical Engineering, Iran University of Science and Technology, Tehran 1684613114, Iran (e-mail: abbas_shiri@iust.ac.ir; shoulaie@iust.ac.ir).

Color versions of one or more of the figures in this paper are available online at http://ieeexplore.ieee.org.

Digital Object Identifier 10.1109/TEC.2012.2190416

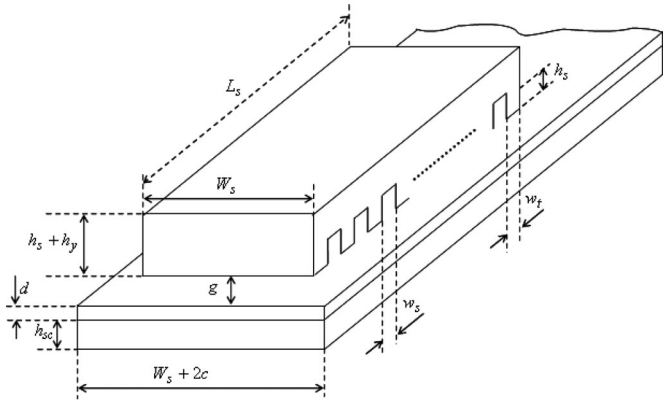

Fig. 1. Structure of SLIM.

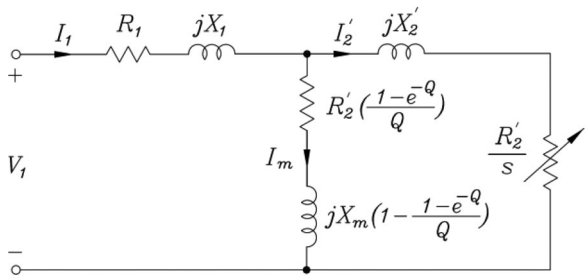

Fig. 2. Equivalent circuit of SLIM.

In the aforementioned equation, σ_w is the conductivity of the conductor used in the primary winding, $l_{\rm ec}$ is the end connection length, W_s primary width, N the per-phase number of turns of the primary winding, and A_w is the cross-sectional area of the conductor.

The primary leakage reactance is given by [29] and [30]:

$$X_1 = 2\mu_0\omega_1[(\lambda_s(1+3/2p)+\lambda_d)W_s/q+\lambda_e l_{\rm ec}]N^2/p \quad (2)$$

where μ_0 is the permeability of the vacuum, p the number of pole pairs, q the number of the slots per pole per phase, ω_1 primary angular frequency, and λ_s, λ_e, and λ_d are the permeances of slot, end connection, and differential, respectively, which are given by the following equations [29]:

$$\lambda_s = h_s(1+3\beta)/(12w_s) \quad (3)$$

$$\lambda_e = 0.3(3\beta-1) \quad (4)$$

$$\lambda_d = 5(g_e/w_s)/[5+4(g_e/w_s)]. \quad (5)$$

In the above equations, β is the pitch factor of the coil. The per-phase magnetizing reactance of the motor is given by [29]

$$X_m = 6\mu_0\omega_1 W_{se}k_w^2 N^2\tau/(\pi^2 p g_e) \quad (6)$$

where k_w is the winding factor, τ the pole pitch, and W_{se} and g_e are the equivalent primary width and the effective air-gap, respectively, and are calculated by the following equations:

$$W_{se} = W_s + g_m \quad (7)$$

$$g_e = (k_c k_l/k_{tm})(1+k_s)g_m. \quad (8)$$

In the aforementioned equations, $g_m = g + d$ is the magnetic air-gap in which g is the air-gap length and d is the secondary aluminum sheet thickness. Also, k_l is air-gap leakage factor, k_c Carter's coefficient, k_{tm} magnetizing reactance factor due to edge effect, and k_s is the secondary saturation factor [29].

For calculation of the secondary resistance, the conductivity of the secondary sheet should be modified. The effective conductivity of the secondary sheet, σ_e is given by [29]

$$\sigma_e = \sigma/k_{\rm sk} \quad (9)$$

in which

$$k_{\rm sk} = \frac{2d}{\delta_s}\left[\frac{\sinh(2d/\delta_s)+\sin(2d/\delta_s)}{\cosh(2d/\delta_s)-\cos(2d/\delta_s)}\right] \quad (10)$$

where δ_s is the depth of penetration of the secondary sheet which can be calculated by

$$\delta_s = [0.5(\pi/\tau)^2 + \mu_0\pi f_1 s\sigma]^{-1/2}. \quad (11)$$

In the above equation, f_1 is the primary supply frequency, τ the motor pole pitch, σ is the conductivity of the secondary sheet that is reduced by the factor $k_{\rm sk}$ because of the skin effect phenomenon. Besides the skin effect, the edge effect reduces the secondary conductivity by the factor k_{tr}. If the latter factor and contribution of the secondary back iron in conduction of the secondary current are taken into account, the effective conductivity is modified to

$$\sigma_{ei} = \frac{\sigma}{k_{\rm sk}k_{tr}} + \frac{\sigma_i\delta_i}{k_{tri}d}. \quad (12)$$

The primary referred secondary resistance is defined as follows [31]:

$$R_2' = X_m/G_e \quad (13)$$

where G_e is modified goodness factor of the motor that is given by [29]

$$G_e = 2\mu_0 f_1\tau^2\sigma_{ei}d/(\pi g_e). \quad (14)$$

In secondary sheet LIMs, the secondary reactance can be neglected [32]. So, $X_2' \approx 0$. Also, due to low value of flux density in the air-gap, the core loss is negligible; so, $R_c \approx 0$.

III. Performance Calculations

In this section, in order to derive analytical equations for efficiency, power factor, and developed thrust, the Duncan equivalent circuit model of LIM is employed [25]. In [20], analytical equations have been derived for efficiency and power factor; however, in calculations, the power loss due to the end effect is supposed to occur prior to air-gap. It is obvious that the power loss due to end effect occurs in the secondary due to eddy currents produced by the end effect. So, the developed air-gap power is defined in such a way that considers this phenomenon (see Fig. 3); thus, the following equation holds:

$$P_{\rm ag} = P_{Ale} + P_{Als} + P_m. \quad (15)$$

In the above equation, P_{Ale} is the power loss due to the end effect, P_{Als} is the secondary ohmic loss, and P_m is the converted

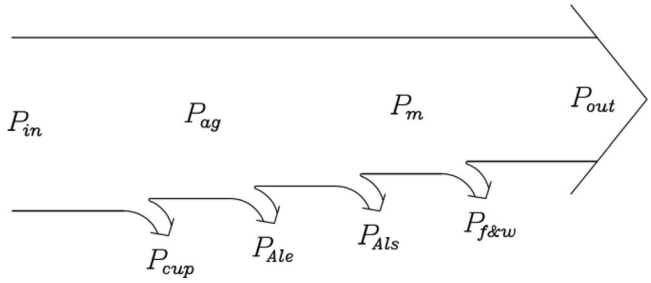

Fig. 3. Power flow in SLIM.

mechanical power. So, considering equivalent circuit of Fig. 2, we can write

$$P_{Ale} = 3R_m I_m^2 \tag{16}$$

$$P_{Als} = 3R_2' I_2'^2 \tag{17}$$

$$P_m = 3\frac{1-s}{s} R_2' I_2'^2. \tag{18}$$

In (16), R_m is the magnetizing branch resistance in the Duncan model that represents the power loss due to end effect and is equal to

$$R_m = R_2'[1 - e^{-Q}]/Q. \tag{19}$$

In the above equation, Q is normalized motor length. The value of Q is obtained by the following equation [25]:

$$Q = L_s R_2'/[(L_m + L_2')V_r] \tag{20}$$

where L_s is the primary length, L_m the magnetizing inductance, L_2' the secondary leakage inductance which is equal to zero for sheet secondary, and V_r is the motor speed. It is seen that the value of Q inversely depends on motor speed, so in high speeds it becomes smaller.

In addition to (15), the air-gap power can be written in terms of developed thrust F_x:

$$P_{\rm ag} = V_s F_x = 2f_1 \tau F_x \tag{21}$$

where V_s is the synchronous speed, f_1 is the primary supply frequency, and τ is the pole pitch of the motor.

The efficiency of the motor is defined as follows:

$$\eta = P_{\rm out}/P_{\rm in} \tag{22}$$

where $P_{\rm out}$ and $P_{\rm in}$ are output and input power of the motor, respectively. Referring to Fig. 2 and replacing proper terms for input and output power, the following equations for efficiency, power factor, and developed thrust are derived:

$$\eta = [F_x 2\tau f_1(1-s) + 3(s-1)R_m I_m^2]/[F_x 2\tau f_1 + 3I_1^2 R_1] \tag{23}$$

$$\cos\varphi = (F_x 2\tau f_1 + 3I_1^2 R_1)/(3I_1 V_1) \tag{24}$$

$$F_x = \frac{3I_1^2 R_2'}{s2\tau f_1}\left[\frac{R_m(R_2'/s + R_m) + X_{m1}^2}{(R_2'/s + R_m)^2 + X_{m1}^2}\right]. \tag{25}$$

In the above equations, s is the motor slip and X_{m1} is the modified magnetizing reactance considering end effect that is equal to

$$X_{m1} = X_m(1 - [1 - e^{-Q}]/Q). \tag{26}$$

It should be mentioned that in deriving the aforementioned equations, the mechanical friction and windage loss of the motor are neglected. Air-gap flux density is given by [29]

$$B_g = \mu_0 J_m \tau/[\pi g_e \sqrt{1 + (sG_e)^2}] \tag{27}$$

where J_m is the amplitude of the equivalent current sheet that is calculated as follows [29], [33]:

$$J_m = 3\sqrt{2} k_w N I_1/(\pi\tau). \tag{28}$$

Using (27), the tooth flux density is obtained by

$$B_t = B_g \tau_s / w_t. \tag{29}$$

IV. Braking Force Due to End Effect

As is known, the longitudinal end effect decreases the air-gap flux density of the SLIM. The final effect of this phenomenon is producing a braking force that is opposite to developed thrust in the air-gap. This braking force can be considered as an external mechanical load. Based on the authors' knowledge, the EEBF has not been considered in design by researchers in the literature. In this section, an analytical equation is derived for the EEBF. The net output force, F_{xo} can be written as follows:

$$F_{xo} = F_x - F_{xe} \tag{30}$$

where F_x is the developed force of the motor in the air-gap and F_{xe} is the EEBF. The developed air-gap power is obtained by (21) and the converted mechanical power can be calculated by the following equation:

$$P_m = V_r F_{xo}. \tag{31}$$

In the above equation, V_r is the motor speed. Using (15)–(18), the converted mechanical power can be written as follows:

$$P_m = (1-s)P_{\rm ag} + (s-1)P_{Ale}. \tag{32}$$

Dividing (32) by $(1-s)P_{\rm ag}$ and using (21) and (31), following relation is derived:

$$F_{xo}/F_x = 1 - P_{Ale}/P_{\rm ag}. \tag{33}$$

Replacing F_{xo} from (30) in the aforementioned equation and using (21) for $P_{\rm ag}$, the braking force produced by the end effect is derived as follows:

$$F_{xe} = P_{Ale}/V_s. \tag{34}$$

Using (16) and (19) and also referring to Fig. 2, the final form of the EEBF is derived as follows:

$$F_{xe} = \frac{3R_2'(R_2'/s)^2[1 - e^{-Q}]}{QV_s[(R_2'/s + R_m)^2 + X_{m1}^2]} I_1^2. \tag{35}$$

It is seen that when the speed of the motor goes up, the value of Q decreases and it cause the EEBF to increase. The reason for the latter is that when Q decreases, the modified magnetizing reactance of the motor [see (26)] decreases too and causes the input current to increase.

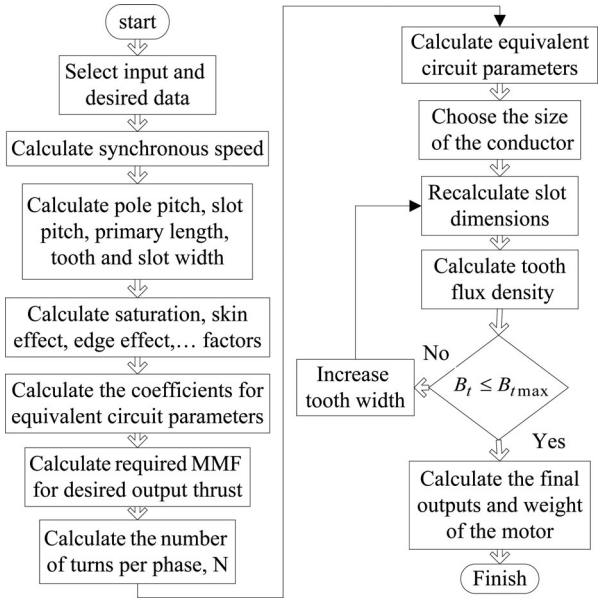

Fig. 4. Flowchart of the SLIM design procedure.

V. Design Procedure

Using (25) and (35) in (30), and doing some mathematical calculations, output thrust can be obtained as follows:

$$F_{xo} = \frac{3I_1^2 R_2'}{s2\tau f_1}\left[\frac{R_m^2 + X_{m1}^2}{(R_2'/s + R_m)^2 + X_{m1}^2}\right]. \tag{36}$$

By replacing motor parameters [see (13), (19), and (26)] in the above equation, the required MMF in order to produce the desired output thrust is obtained as follows:

$$\text{MMF} = NI_1 = \sqrt{\frac{s2\tau f_1 F_{xo}}{3K_{R_2'}}\frac{(K_{R_2'}/s + K_{R_m})^2 + K_{X_{m1}}^2}{K_{R_m}^2 + K_{X_{m1}}^2}} \tag{37}$$

where the following equations are used:

$$R_2' = K_{R_2'} N^2 \tag{38}$$

$$R_m = K_{R_m} N^2 \tag{39}$$

$$X_{m1} = K_{X_{m1}} N^2. \tag{40}$$

Referring to per-phase equivalent circuit (see Fig. 2), the following equation holds for the per-phase number of turns of the primary:

$$V_1 = K_z N^2 I_1 \tag{41}$$

where $Z = K_z N^2$ is the per-phase input impedance of the motor, in which constant K_Z is equal to

$$K_z = K_{R_1} + jK_{X_1} + (K_{R_m} + jK_{X_{m1}}) \,||\, (K_{R'2}/s)\,. \tag{42}$$

By calculation of the number of turns using (41), the calculation of the equivalent circuit parameters and other motor outputs are straightforward. Flowchart of the SLIM design procedure is illustrated in Fig. 4.

TABLE I
Specification of the Investigated Motor

Input phase voltage, V	220
Supply frequency, Hz	166
Number of pole pairs,(p)	4
Number of slots/pole/phase(q)	3
Primary width, mm	148.3
Thickness of the secondary sheet, mm	2.5
Primary current density, *A/mm²*	6
Air-gap length, mm	5.1

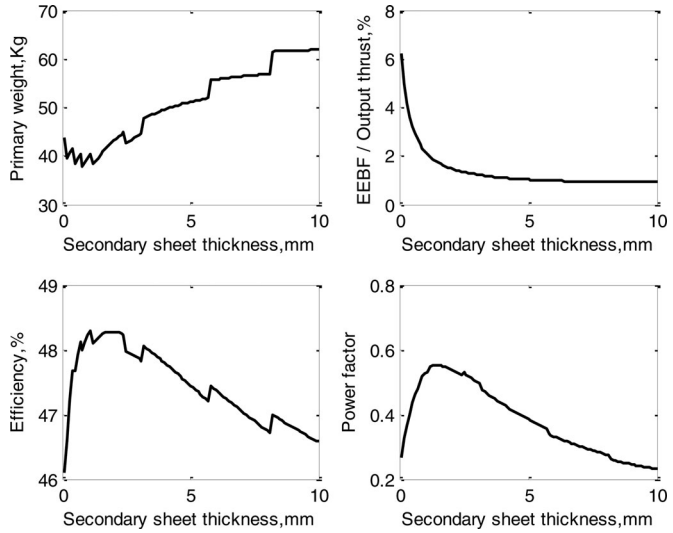

Fig. 5. Motor outputs versus the secondary sheet thickness.

VI. Simulation Results and Performance Analysis

Different design variables affect motor performance in different ways. To investigate the effect of design variables such as the secondary sheet thickness, the air-gap length, the supply frequency, the primary width, etc. on the motor performance, the designed SLIM is simulated using MATLAB software. The reaction of the motor to independent design variables is important in optimization problem. In these simulations, the motor is designed to have (1000 ± 100)N output thrust in motor speed of $V_r = 15$ m/s.

Other variables that are fixed during the design in Figs. 5–12 are given in Table I (in each figure only one of them is being changed).

In Fig. 5, the effect of the secondary sheet (Aluminum) thickness on the motor outputs such as primary weight, the ratio of EEBF to output thrust, efficiency, and power factor are illustrated. In the figure, other independent variables are kept constant. As is seen in the figure, by increasing the aluminum thickness, the primary weight of the motor increases; while, the ratio of the EEBF to output thrust decreases. Also, the power factor and the efficiency increase until they reach a maximum value and then decrease. As a result, to select a proper value for aluminum thickness, there should be a compromise between different outputs such as efficiency, EEBF/output thrust and power factor. The cost of the aluminum should be added to mentioned challenges, because increasing the aluminum sheet thickness increases the amount of the aluminum. It is seen that

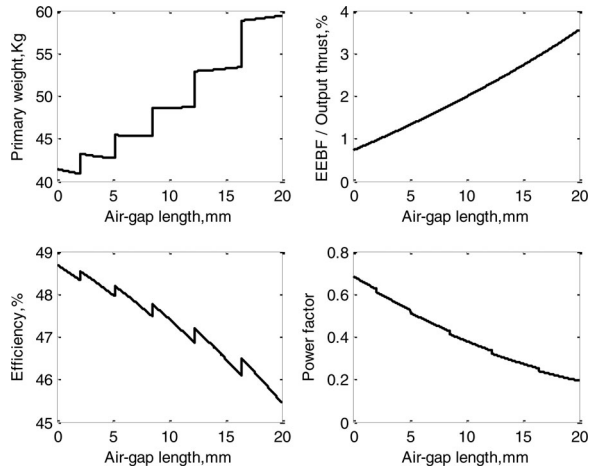

Fig. 6. Motor outputs versus the air-gap.

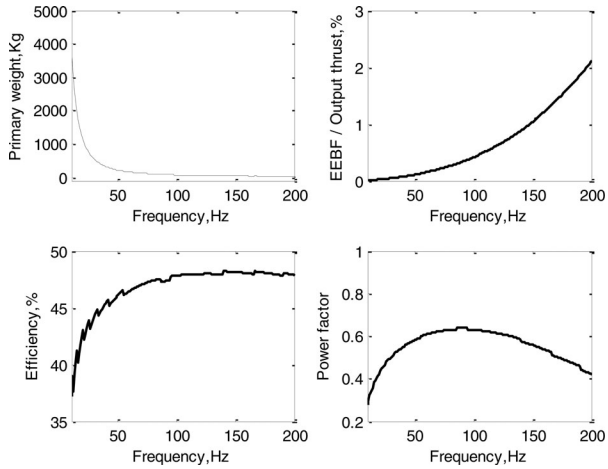

Fig. 7. Motor outputs versus the input frequency.

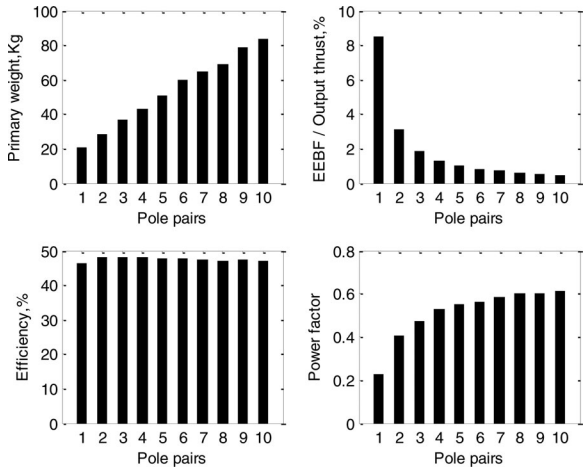

Fig. 8. Motor outputs versus number of pole pairs.

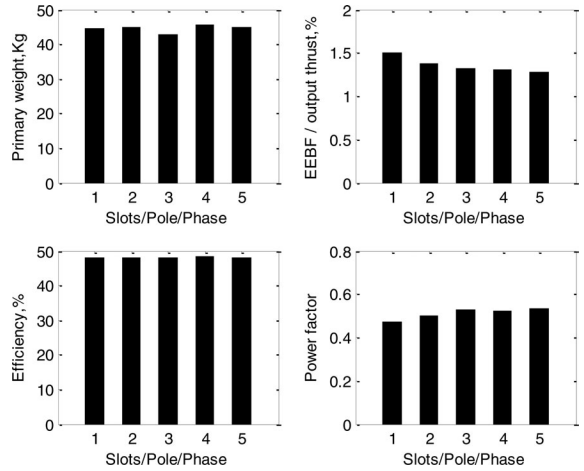

Fig. 9. Motor outputs versus number of slots per pole per phase.

there are some jumps on the curves in the figure. These jumps are because of rounding the number of turns per coil to nearest integer in design process. The variation of the outputs versus the air-gap length is shown in Fig. 6. It is seen that increasing the air-gap length increases the primary weight to produce constant output thrust. Also, the EEBF/output thrust increases as air-gap length increases. On the other hand, efficiency and power factor decrease as the air-gap is increased. As a result, in design process, the air-gap should be chosen as short as possible to maximize efficiency and power factor, at the same time to minimize weight and EEBF. It should be mentioned that in some applications such as high-speed traction motors, minimum value of the air-gap length is limited. The jumps in Figs. 6 and 7–12 are also because of rounding the number of turns per coil to nearest integer in design process. In many applications, voltage source inverters provide input voltage. Therefore, the input voltage frequency can be easily varied. So, the effect of variation of the frequency on the performance of the motor is investigated. Fig. 7 shows the simulation results of the motor by changing input frequency. As is seen in the figure, increasing the frequency decreases the primary weight; at the same time increases the EEBF. The efficiency is increased by increasing frequency; although, in high frequencies the changes of efficiency become smaller and then the latter decreases. Also, the power factor increases until frequency of about 90 Hz and then decreases. Fig. 8 illustrates the variation of the motor outputs versus number of pole pairs. Increasing the pole number increases the motor length in constant frequency, synchronous speed, and primary width, which leads to the increment of the primary weight. On the other hand, EEBF reduces by increasing the pole number. In addition, increasing the number of poles has small effect on efficiency; however, it increases the power factor. As seen in Fig. 9, increasing the number of slots/pole/phase has negligible effect on primary weight and efficiency. However, it slightly decreases the EEBF and increases power factor. Increasing the primary current density with constant output thrust decreases the primary wire cross-section and increases the primary resistance of the motor. So, it causes the primary weight and efficiency to reduce (see Fig. 10). It also increases the power factor; however, it has no effect on EEBF. In Fig. 11, increasing the primary width with constant motor length increases the primary weight and power factor, at the same time it decreases EEBF and efficiency, although the changes in efficiency are small. Finally, increasing the ratio of slot width to slot pitch decreases the primary weight and increases the EEBF and power factor, while having negligible effect on efficiency (see Fig. 12). According

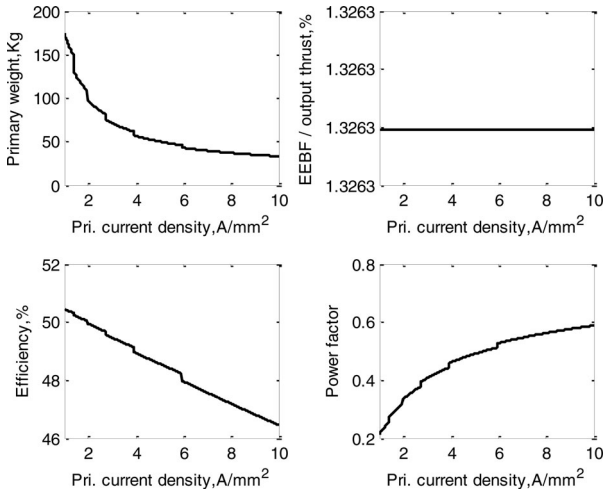

Fig. 10. Motor outputs versus primary current density

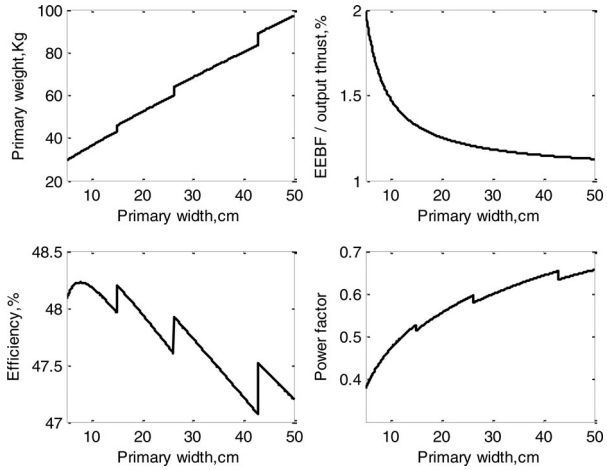

Fig. 11. Motor outputs versus primary width.

to the aforementioned explanations and considering the application of the motor and its limitations, one can develop the design in a way that the motor can produce optimum outputs. In the next section, using genetic algorithm, the design is optimized considering all effective variables of the motor.

VII. Genetic Algorithm-Based Design Optimization

In an optimization problem, if independent variables are defined as $x = (x_1, x_2, ..., x_n)$, the goal is to find a vector x such that optimizes the predefined function $f(x)$ under some constraints. As seen in the previous section, to design an SLIM, different variables can be chosen for vector x. Considering the results of investigations performed, in this paper, variables of vector x are chosen as follows: primary input frequency f_1, number of pole pairs p, number of slots per pole per-phase q, primary current density J, primary width W_s, secondary sheet thickness d, motor slip s, slot width to slot pitch ratio w_s/τ_s, and the mechanical clearance g. In addition, tooth flux density and the ratio of primary width to pole pitch are applied as

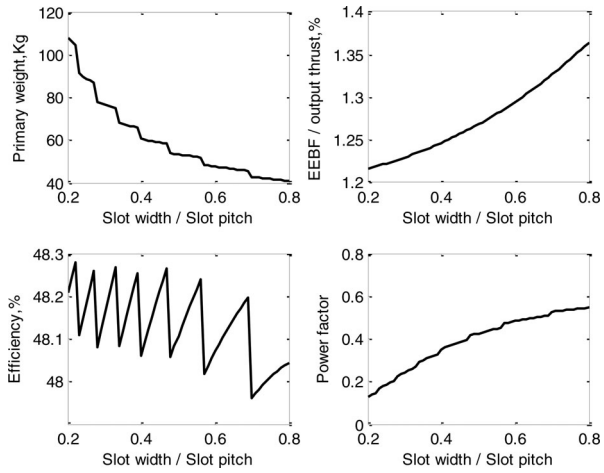

Fig. 12. Motor outputs versus slot width/slot pitch.

TABLE II
Design Variable Constraints

Parameter	Minimum value	Maximum value
Primary current density, A/mm^2	3	6
Primary width, mm	50	300
Secondary sheet thickness, mm	1	5
Slip	0.1	0.5
Air gap length, mm	5	20
Number of pole pairs	1	4
Slot width / Slot pitch	0.4	0.7
Slots/Pole/Phase	1	3
Frequency, Hz	1	200

optimization constraints:

$$B_t \leq 1.6 \tag{43}$$

$$0.5 \leq W_s/\tau \leq 4. \tag{44}$$

Other variable constraints applied to the design are listed in Table II.

To achieve the optimization goal, different output parameters of the motor can be considered as objective function. The aim of this paper is to minimize end-effect force and primary weight, as well as to maximize the efficiency and power factor, simultaneously. So, the objective function is defined as follows:

$$f(x) = \frac{\eta(x)^{K_1} \times \text{P.F.}(x)^{K_2}}{[\text{Primary weight}(x)]^{K_3} \times F_{xe}(x)^{K_4}} \tag{45}$$

where x is the optimization variables vector and K_i $(i = 1...4)$ can be chosen as 0 or 1. The rated specifications of the motor are the same as those used in previous section. In this paper, genetic algorithm is employed for optimization. The genetic algorithm is a method that searches among different variable values and finds a set of parameters to optimize the objective function [34]. The optimization is done for different objective functions using (45). In the first step, $K_1 = K_2 = 1$, $K_3 = K_4 = 0$. It means that only the efficiency and power factor are optimized. In the next step, $K_1 = K_2 = K_3 = 1, K_4 = 0$. In the third step, $K_1 =$

TABLE III
OPTIMIZED MOTORS SPESIFICATIONS

Specification	Optimum values ($K_1 = K_2 = 1$, $K_3 = K_4 = 0$)	Optimum values ($K_1 = K_2 = K_3 = 1$, $K_4 = 0$)	Optimum values ($K_1 = K_2 = K_4 = 1$, $K_3 = 0$)	Optimum values ($K_1 = K_2 = 1$, $K_3 = K_4 = 1$)
Primary current density, A/mm^2	3	6	6	6
Primary width, mm	300	123.7	300	148.3
Secondary sheet thickness, mm	2.5	1.5	2.5	2.5
Air gap length, mm	5.1	5.2	5.1	5.1
Slip	0.25	0.4	0.5	0.48
Number of pole pairs	4	2	4	4
Number of slots/pole/phase	3	3	3	3
Frequency, Hz	22.5	124.5	58	166
Number of turns per phase	156	72	144	108
Phase input current, A	48.57	88.86	61.28	82.19
Motor length(L_s), m	3.5827	0.4050	2.0855	0.7025
Tooth width, mm	27.2	3.3	16.5	2.9
Slot width, mm	22.2	7.8	12.2	6.8
Slot width to slot pitch ratio	0.45	0.7	0.43	0.7
Tooth flux density(B_t), T	0.28	1.57	0.16	0.65
Efficiency, %	66.02	53.95	43.28	47.96
Power factor	0.7662	0.4431	0.7867	0.5260
Primary weight, Kg	983.75	26.81	365.40	42.7057
EEBF, N	27.64	57.69	6.82	12.10
Output thrust, N	1081.1	934.61	918.04	912.26
(EEBF/output thrust), %	2.56	6.17	0.74	1.33
Objective function	0.5059	0.0089	0.0500	4.8823×10^{-4}

$K_2 = K_4 = 1$, $K_3 = 0$, and finally, all outputs are optimized simultaneously: so, $K_1 = K_2 = K_1 = K_2 = 1$.

The optimization design results are shown in Table III. The design is done with constant motor speed of 15 m/s and output thrust of 1000 ± 100 N. In first design case, only efficiency and power factor are optimized. Regarding that there is no limitation on weight, the dimensions of the motor are high and the input frequency is comparatively low. On the other hand, the primary current density is 3 A/mm^2 that leads to high efficiency. In the second case ($K_1 = K_2 = K_3 = 1$, $K_4 = 0$), in addition to efficiency and power factor, the primary weight is optimized too. The results show that the dimensions of the motor are reduced to assure minimum weight (26.81 kg), while the primary current density is 6 A/mm^2; so, the efficiency is reduced, in this case. On the other hand, the braking force caused by end effect is increased (57.69 N) because of the reduced number of poles. In the next case, the EEBF is optimized, simultaneously with efficiency and power factor, while the primary weight is not considered in optimization. As seen in Table III, the dimensions of the motor is increased that leads to high primary weight, while the EEBF is reduced considerably (6.82 N). In the last case ($K_1 = K_2 = K_3 = K_4 = 1$), all of the four outputs are optimized, simultaneously. In this case, the dimensions of the motor are comparatively low but higher than their counterparts in case 2. Also, the EEBF in this case is lower than those in cases 1 and 2. It should be mentioned that if the EEBF is not considered, as in case 2 of Table III, the optimal designs with low number of pole pairs are obtained. So, as shown in the previous section, the number of pole pairs has a determinant effect on the braking force produced by the end effect.

As is known, in different runs, different results are obtained by genetic algorithm in an optimization problem [34]. In order to examine the effectiveness of the genetic algorithm in optimization of the SLIM, the results of 20 runs for the design case 4 of Table III are compared. The average values for the efficiency, the power factor, the primary weight and the EEBF as well as objective function are shown in Table IV. Regarding the objective function, case 4 in Table III is the best optimal design among 20 mentioned designs. As seen in Table IV, the averaged design results obtained by 20 different runs are close enough to their counterparts in Table III, confirming the effectiveness of the genetic algorithm in optimization of SLIM.

VIII. FINITE ELEMENT ANALYSIS

In this paper, based on the Duncan equivalent circuit model, analytical equations are derived for the output thrust, efficiency, and the EEBF. Optimization of the design as well as minimization of the EEBF at constant speed is performed using proposed output equations. So, the effectiveness of the design mainly depends on the validity of the developed model. To validate the model and to confirm the results of the optimization, 2-D and 3-D FEMs are employed in this paper. In this section, the optimized design case 4 with limited pole pairs is simulated using 2-D and 3-D FEM (pole pairs are limited to 2). Computer hardware limitations and avoiding the complexity of the model implemented in the FEM are the only reasons for limiting the pole numbers. The specifications of the optimized design example with limited pole pairs that is called "case 5" hereafter, are shown in Table V. In this design, all of the four outputs are optimized, simultaneously ($K_1 = K_2 = K_3 = K_4 = 1$). Fig. 13

TABLE IV
OPTIMIZED MOTOR PARAMETER VALUES IN 20 DIFFERENT RUNS ($K_1 = K_2 = K_3 = K_4 = 1$)

	Efficiency, %	Power factor	Primary weight, Kg	EEBF, N	Output thrust, N	Objective function
Average value	47.23	53.72	46.99	11.65	914.88	4.6584×10^{-4}

TABLE V
OPTIMIZED MOTOR PARAMETER VALUES FOR FEM SIMULATIONS

Specification	Optimum values ($K_1=K_2=1$, $K_3=K_4=1$)
Phase input voltage, V	220
Motor speed, m/s	15
Primary current density, A/mm^2	6
Primary width, mm	130
Secondary sheet thickness, mm	2.0
Air gap length, mm	5.1
Slip	0.5
Number of pole pairs	2
Number of slots/pole/phase	3
Frequency, Hz	146.5
Number of turns per phase	72
Phase input current, A	93.65
Motor length(L_s), m	0.4138
Tooth width, mm	2.9
Slot width, mm	6.8
Slot width to slot pitch ratio	0.7
Slot depth, mm	39.3
Tooth flux density(B_t), T	1.1
Efficiency, %	46.46
Power factor	0.4884
Primary weight, Kg	29.34
EEBF, N	28.46
Output thrust, N	934.98
Objective function	2.7176×10^{-4}

shows the flux paths in the different parts of the motor as it moves in x-direction (2-D FEM). It is seen that the flux lines are denser in exit end of the motor. To investigate the edge effect on the performance of the SLIM, the latter is simulated using 3-D FEM. Flux density distribution in the primary core is illustrated in Fig. 14. The maximum flux density in different parts of the motor is limited to 1.88 T. The distributions of the flux density in the secondary sheet as well as the secondary current are shown in Figs. 15 and 16, respectively. It should be mentioned that the flux density in the secondary sheet can be a representative of the air-gap flux density. It is seen in Fig. 15 that the maximum flux density in the secondary sheet and consequently in the air-gap is about 0.24 T. The efficiency, the power factor, and the output thrust are calculated using the 2-D and 3-D FEM. The analytical calculation results are compared with FEM results in Table VI. As seen in this table, the efficiency obtained by 2-D and 3-D FEM are lower than that of obtained by analytical design. It may be partly because of neglecting iron loss in an analytical model that is considered in FEM. Also, the thrust and power factor obtained by the 3-D FEM are in good agreement with the analytical results. In addition, they are slightly lower than those of obtained by the 2-D FEM. This is because of the edge effect phenomenon that is considered in the 3-D FEM. Edge effect causes the secondary resistance to increase and the magnetizing reactance to decrease [29].

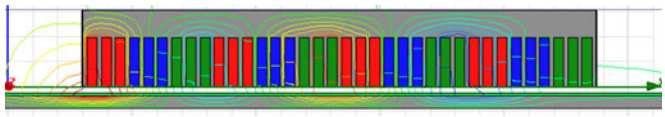

Fig. 13. Flux paths in the moving SLIM.

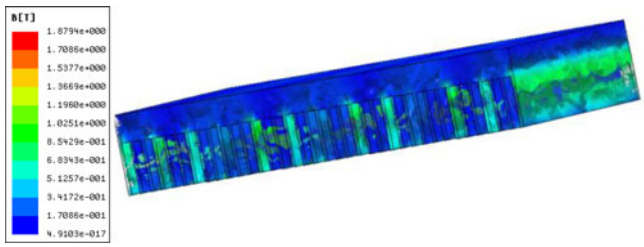

Fig. 14. Flux density distribution in the primary core.

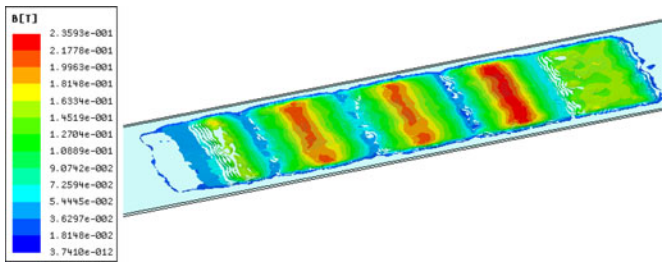

Fig. 15. Flux density distribution in the secondary sheet.

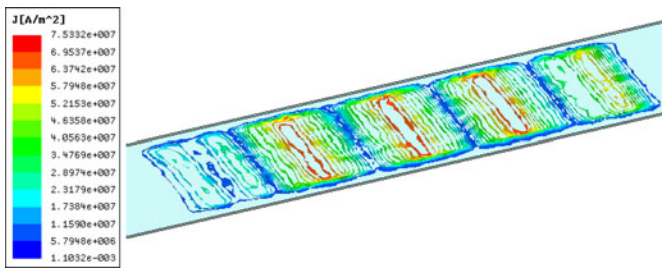

Fig. 16. Current distribution in the secondary sheet.

TABLE VI
CALCULATION AND FEM RESULTS

parameter	Analytical	2-D FEM	3-D FEM
Efficiency, %	46.46	43.27	43.21
Power factor	0.4884	0.5211	0.4932
Output thrust, N	934.98	942.5	936.4

IX. THERMAL ANALYSIS

As the air-gap length is comparatively high (5.1 mm), the heat transfer between primary and secondary can be neglected [35]. So, the thermal behavior of them can be analyzed separately.

TABLE VII
SLIM SPECIFICATION FOR THERMAL ANALYSIS

Thermally equivalent primary current, A	78.16
Primary equivalent copper loss, W	460.14
Primary back-iron weight, Kg	9.19
Teeth weight, Kg	4.92
Primary iron loss, W	83.27

A. Secondary Thermal Analysis

In transportation applications, between the stop stations, the velocity of the motor is close to the steady-state speed. So, the secondary does not have enough time to reach high temperatures. However, in stop stations the secondary can be overheated. The thermal design of the secondary of SLIM is based on the number of vehicles that start moving from same place at stop station [35]. The minimum interval between two successive vehicles should be such that the secondary does not exceed the thermal limit.

B. Primary Thermal Analysis

To analyze the thermal behavior of the primary of the SLIM, for transportation applications, the equivalent thermal loss of the primary should be calculated. So, the equivalent primary current is obtained as follows [35]:

$$I_{e\text{-th}} = I_n \sqrt{\frac{(t_a + t_d)}{T}\left(\frac{I_s}{I_n}\right)^2 + \frac{t_c}{T}\left(\frac{I_n}{I_n}\right)^2 + \frac{t_s}{T}\left(\frac{0}{I_n}\right)^2} \tag{46}$$

where t_a and t_d are acceleration and deceleration time, respectively, t_c cruising time between two stations, t_s stop time at station, T the time which motor travels between two stations, I_n the nominal input current, and I_s is the input current at starting. It should be mentioned that the current during acceleration and deceleration period is assumed to be I_s, for convenience. The equivalent primary copper loss is equal to

$$P_{e\text{-cup}} = 3R_1 I_{e\text{-th}}^2. \tag{47}$$

As the primary width of the motor is approximately equal to end connection length, about half of the aforementioned loss is distributed in active part of the SLIM and half other in the end connection. In Table VII, the thermal equivalent primary current, the equivalent primary copper losses, as well as primary iron losses are given. The iron type *M270-35 A5* is considered for primary.

FEM Simulations: To investigate the distribution of the temperature on different parts of the SLIM, the FEM is employed. To model the heat exchange between the SLIM and the air, the convection heat transfer coefficients for different surfaces of the SLIM should be determined. The relations for these coefficients can be found in thermal analysis handbooks [36], [37]. The convection heat transfer coefficients for different surfaces of the SLIM are calculated as in Table VIII.

With the obtained convection heat transfer coefficients, the SLIM is simulated using Flux software. The primary winding and the iron core are considered as thermal sources. In simulations, the ambient temperature is assumed to be 25 °C. The

TABLE VIII
CONVECTION HEAT TRANSFER COEFFICIENTS BETWEEN THE SLIM AND THE AIR

Front surface, $W/(m^2K)$	61.75
Back surface, $W/(m^2K)$	110.5
Peripheral surfaces, $W/(m^2K)$	32.2
Upper surface for forced cooling system, $W/(m^2K)$	152.4

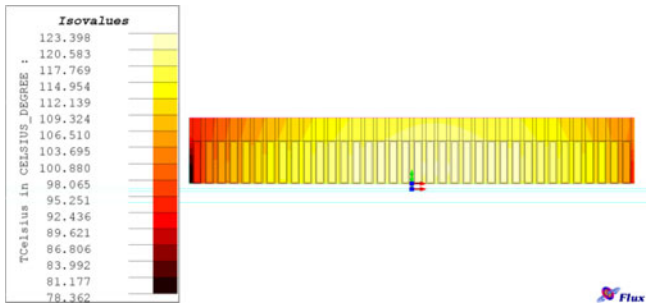

Fig. 17. Distribution of the temperature on different parts of the SLIM.

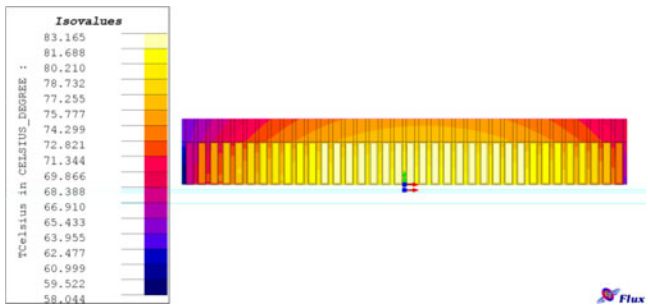

Fig. 18. Distribution of the temperature on different parts of the SLIM with forced cooling system.

distribution of the temperature on different parts of the SLIM is illustrated in Fig. 17. It is seen that the hottest temperature is 123.4 °C that is occurs in about the middle slots of the motor. It is also clear that the temperature of the backside of the motor is lower than that of front side. It is because of the high value of the convection heat transfer coefficient that is obtained for a backside surface. It seems that using insulation class F suffices for windings in slots. If a forced cooling system such as a simple fan is used, the convection heat transfer coefficients of the surfaces increase. As an example the calculation is carried out for upper side of the motor that the convection heat transfer coefficient is obtained as $152.4\mathrm{W}/(\mathrm{m}^2\mathrm{K})$. With the obtained coefficient, the FEM simulation results are shown in Fig. 18. It is seen that the hottest temperature decreases from 123.4 °C in the previous case without fan to 83.17 °C in this case.

X. CONCLUSION

A simple and applicable procedure based on the Duncan equivalent circuit model is proposed to design the single-sided LIM. All phenomena such as longitudinal end effect, iron saturation, transverse edge effect, and skin effect are considered in design. An analytical equation is derived to model braking force

produced by the end effect. Also, based on the defined air-gap power, equations for the efficiency, and power factor as well as output thrust are analytically derived. A multiobjective optimization method is employed to maximize the power factor and efficiency and simultaneously, to minimize the primary weight and the EEBF for high speed SLIMs. The results show that EEBF can be considerably minimized by appropriate selection of the motor parameters, especially the number of poles. The 2-D and 3-D FEM is used to confirm the precision of the derived equations for outputs and the effectiveness of the optimization method. The FEM results, in which the end effect is taken into account, are in good agreement with the analytical results. This confirms the validity of the proposed analytical equations and optimal design.

REFERENCES

[1] E. R. Laithwaite and S. A. Nasar, "Linear-motion electrical machines," *Proc. IEEE*, vol. 58, no. 4, pp. 531–542, Apr. 1970.

[2] D. H. Im, S. C. Park, and J. W. Im, "Design of single-sided linear induction motor using the finite element method and SUMT," *IEEE Trans. Magn.*, vol. 29, no. 2, pp. 1762–1766, Mar. 1993.

[3] S. Nonaka, "Investigation of equivalent circuit quantities and equations for calculation of characteristics of single-sided linear induction motors (LIM)," *Elect. Eng. Jpn.*, vol. 117, no. 2, pp. 107–121, 1996.

[4] S. Nonaka, "Investigation of equations for calculation of secondary resistance and secondary leakage reactance of single-sided linear induction motors," *Elect. Eng. Jpn.*, vol. 122, no. 1, pp. 60–67, 1998.

[5] R. C. Creppe, J. A. C. Ulson, and J. F. Rodrigues, "Influence of design parameters on linear induction motor end effect," *IEEE Trans. Energy Convers.*, vol. 23, no. 2, pp. 358–362, Jun. 2008.

[6] S. G. Lee, H. Lee, S. Ham, C. Jin, H. Park, and J. Lee, "Influence of the construction of secondary reaction plate on the transverse edge effect in linear induction motor," *IEEE Trans. Magn.*, vol. 45, no. 6, pp. 2815–2818, Jun. 2009.

[7] B. Lee, D. Koo, and Y. Cho, "Investigation of linear induction motor according to secondary conductor structure," *IEEE Trans. Magn.*, vol. 45, no. 6, pp. 2839–2842, Jun. 2009.

[8] D. Hall, J. Kapinski, M. Krefta, and O. Christianson, "Transient electromechanical modeling for short secondary Linear induction machines," *IEEE Trans. Energy Convers.*, vol. 23, no. 3, pp. 789–795, Sep. 2008.

[9] S. Nonaka and T. Higuchi, "Elements of linear induction motor design for urban transit," *IEEE Trans. Magn.*, vol. 23, no. 5, pp. 3002–3004, Sep. 1989.

[10] S. Yoon, J. Hur, and D. Hyun, "A method of optimal design of single-sided linear induction motor for transit," *IEEE Trans. Magn.*, vol. 33, no. 5, pp. 4215–4217, Sep. 1997.

[11] W. Xu, J. Zhu, L Tan, Y. Guo, S Wang, and Y. Wang, "Optimal design of a linear induction motor applied in transportation," in *Proc. IEEE Int. Conf. Ind. Tech.*, 2009, pp. 1–6.

[12] D. Yumei and J. Nenggiang, "Research on characteristics of single-sided linear induction motors for urban transit," in *Proc. IEEE Int. Con. Elect. Mach. Syst.*, 2009, pp. 1–4.

[13] S. Osawa, M. Wada, M. Karita, D. Ebihara, and T. Yokoi, "Light-weight type linear induction motor and its characteristics," *IEEE Trans. Magn.*, vol. 28, no. 4, pp. 3003–3005, Sep. 1992.

[14] M. Kitamura, N. Hino, H. Nihei, and M. Ito, "A direct search shape optimization based on complex expressions of 2-dimentional magnetic fields and forces," *IEEE Trans. Magn.*, vol. 34, no. 5, pp. 2845–2848, Sep. 1998.

[15] B. Laporte, N. Takorabet, and G. Vinsard, "An approach to optimize winding design in linear induction motors," *IEEE Trans. Magn.*, vol. 33, no. 2, pp. 1844–1847, Mar. 1997.

[16] T. Mishima, M. Hiraoka, and T. Nomura, "A study of the optimum stator winding arrangement of LIM in maglev systems," *IEEE Int. Conf. Electr. Mach. Drives*, pp. 1238–1242, May 2005.

[17] Isfahani, A. Hassanpour, H. Lesani, and B. M. Ebrahimi, "Design optimization of linear induction motor for improved efficiency and power factor," in *Proc. IEEE Int. Conf. Electr. Mach. Drives*, May 2007, pp. 988–991.

[18] A. Hassanpour Isfahani, B. M. Ebrahimi, and H. Lesani, "Design optimization of a low-speed single-sided linear induction motor for improved efficiency and power factor," *IEEE Trans. Magn.*, vol. 44, no. 2, pp. 266–272, Feb. 2008.

[19] C. Lucas, Z. Nasiri-Gheidari, and F. Tootoonchian, "Application of an imperialist competitive algorithm to design of linear induction motor," *Elsevier Energy Convers. Manag.*, vol. 51, pp. 1407–1411, 2010.

[20] A. Z. Bazghaleh, M. R. Naghashan, and M. R. Meshkatoddini, "Optimum design of single-sided linear induction motors for improved motor performance," *IEEE Trans. Magn.*, vol. 46, no. 11, pp. 3939–3947, Nov. 2010.

[21] J. F. Gieras, G. E. Dawson, and A. R. Easthan, "A new longitudinal end effect factor for linear induction motor," *IEEE Trans. Energy Convers.*, vol. 2, no. 1, pp. 152–159, Mar. 1987.

[22] R. C. Creppe, J. A. C. Ulson, and J. F. Rodrigues, "Influence of design parameters on linear induction motor end effect," *IEEE Trans. Energy Convers.*, vol. 23, no. 2, pp. 358–362, Jun. 2008.

[23] J. Lu and W. Ma, "Research on end effect of linear induction machine for high-speed industrial transportation," *IEEE Trans. Plasma Sci.*, vol. 39, no. 1, pp. 116–120, Jan. 2011.

[24] T. Yang, L. Zhou, and L. Li, "Influence of design parameters on end effect in long primary double-sided linear induction motor," *IEEE Trans. Plasma Sci.*, vol. 39, no. 1, pp. 192–197, Jan. 2011.

[25] J. Duncan, "Linear induction motor-equivalent circuit model," *IEE Proc. Electr. Power Appl.*, vol. 130, no. 1, pp. 51–57, 1983.

[26] W. Xu, J. G. Zhu, Y. Zhang, Y. Li, Y. Wang, and Y. Guo, "An improved equivalent circuit model of a single-sided linearinduction motor," *IEEE Trans. Veh. Techol.*, vol. 59, no. 5, pp. 2277–2289, Jun. 2010.

[27] W. Xu, J. G. Zhu, Y. Zhang, Z. Li, Y. Li, Y. Wang, Y. Guo, and W. Li, "Equivalent circuits for single-sided linear induction motors," *IEEE Trans. Ind. Appl.*, vol. 46, no. 6, pp. 2410–2423, Nov./Dec. 2010.

[28] W. Xu, G. Sun, G. Wen, Z. Wu, and P. K. Chu, "Equivalent circuit derivation and performance analysis of a single-sided linear induction motor based on winding function theory," *IEEE Trans. Veh. Techol.*, 2012.

[29] I. Boldea and S. A. Nasar, *Linear Motion Electromagnetic Devices*. New York: Taylor & Francis, 2001.

[30] S. A. Nasar and I. Boldea, *Linear Electric Motors*. Englewood Cliffs, NJ: Prentice-Hall, 1987.

[31] E. R. Laithwaite, *Induction Machines for Special Purposes*. London, U.K: George Newnes Limited, 1996.

[32] R. M. Pai, I. Boldea, and S. A. Nasar, "A complete equivalent circuit of a linear induction motor with sheet secondary," *IEEE Trans. Magn.*, vol. 24, no. 1, pp. 639–654, Jan. 1988.

[33] J. F. Gieras, *Linear Induction Drives*. New York: Oxford Univ. Press, 1994.

[34] S. Sumathi and P. Surekha, *Computational Intelligence Paradigms: Theory and Applications Using MATLAB*. New York: Taylor & Francis, 2010.

[35] I. Boldea and S. A. Nasar, *Linear Motion Electromagnetic Systems*. New York: Wiley, 1985.

[36] T. L. Bergman, A. S. Lavine, D. P. Dewitt, and F. P. Incropera, *Introduction to Heat Transfer*, 6th ed. New York: Wiley, 2011.

[37] J. P. Holman, *Heat Transfer*, 8th ed. New York: McGraw-Hill, 2001.

Abbas Shiri (S'10) was born in Hashtrood, Iran, in 1980. He received the B.Sc. and M.Sc. degrees both in electrical engineering from the Iran University of Science and Technology, Tehran, Iran, in 2004 and 2006, respectively. He is currently working toward the Ph.D. degree in electrical engineering at the same university.

His areas of research interests include linear electric machines, electromagnetic systems and actuators, electrical machine design, and modeling and power electronics and drives.

Abbas Shoulaie was born in Isfahan, Iran, in 1949. He received the B.Sc. degree from the Iran University of Science and Technology (IUST), Tehran, Iran, in 1973, and the M.Sc. and Ph.D. degrees in electrical engineering from Universite Montpellier II, Montpellier, France, in 1981 and 1984, respectively.

He is a Professor in the Department of Electrical Engineering, IUST. He is the author of more than 100 journal and conference papers in the field of power electronics, electromagnetic systems, electrical machine, linear machine, and HVdc.